LETTER • OPEN ACCESS

Combined, table-top extreme-ultraviolet ellipsometry and polarimetry for studying ultrafast processes in matter

Journal of Physics: Photonics

OPEN ACCESS

RECEIVED
6 September 2025

REVISED
21 November 2025

ACCEPTED FOR PUBLICATION
5 December 2025

PUBLISHED
18 December 2025

LETTER

Combined, table-top extreme-ultraviolet ellipsometry and polarimetry for studying ultrafast processes in matter

Lénárd Gulyás Oldal[1,*], Barnabás Gilicze[1], Tamás Bartyik[1], Dániel Kiss[1], Michele Devetta[2], Gabriele Zeni[3], Fabio Frassetto[3], Luca Poletto[3], Tamás Csizmadia[1] and Balázs Major[1,4]

[1] ELI ALPS, ELI-HU Non-profit Ltd, Wolfgang Sandner utca 3., 6728 Szeged, Hungary
[2] National Research Council, Institute for Photonics and Nanotechnologies, Piazza Leonardo da Vinci 32, 20133 Milano, Italy
[3] National Research Council, Institute for Photonics and Nanotechnologies, Via Trasea 7, 35131 Padova, Italy
[4] Department of Optics and Quantum Electronics, University of Szeged, Dóm tér 9., 6720 Szeged, Hungary
[*] Author to whom any correspondence should be addressed.

E-mail: lenard.gulyas@eli-alps.hu

Keywords: polarization, ellipsometry, reaction microscope, polarimeter, high-harmonics

Supplementary material for this article is available online

Abstract

We demonstrate the characterization of the complete polarization state of broadband extreme-ultraviolet radiation produced via high-harmonic generation in a gas target, measured with a double-stage polarimeter and a reaction microscope. The ellipsometric parameters of the reflective optics used in the polarimeter—meaning the extinction ratios and phase shift—were determined simultaneously. The results serve as a basis for table-top extreme-ultraviolet polarimetric and ellipsometric measurements, allowing ultrafast studies of polarization-sensitive matter, which require exact knowledge of the polarization state of the ionizing radiation.

1. Introduction

The continuous development and unique properties of coherent extreme-ultraviolet (XUV) light sources have made them the most popular tool for the investigation of the fundamental symmetry and magnetization properties of matter [1–3]. One widespread method to produce such radiation is based on a strongly nonlinear frequency up-conversion technique, called high-harmonic generation (HHG) of a fundamental laser field emitting ultrashort pulses [4, 5]. During HHG, the femtosecond-long laser pulses are focused to a target material, which can be solid [6], liquid [7] or crystalline semiconductor material [8]. However, the most commonly used target for HHG is gaseous [9], where laser pulses produce odd-order high-harmonics of the driving laser field resulting in distinct frequency peaks in a broadband XUV spectrum, and achieving attosecond duration temporal evolution [9]. A well-known feature of the process is the inheritance of certain properties of the generating field, such as the spectral characteristics [10–12] and the polarization state [13].

As XUV light sources are indispensable in studies of ultrafast processes happening on the attosecond time scale, there has been a dire need for the complete characterization of their radiation [14–16]. For example, measuring the flux or investigating the spectral features of an XUV source are routine characterization steps before the utilization of their radiation. However, efforts to determine their polarization state with transmissive polarization retarders encounters challenges due to the short attenuation length and lack of birefringent materials in this wavelength range.

In recent decades, a large number of experimental techniques have been developed to determine the exact polarization state of XUV light sources. One of these methods is based on the investigation of photoelectron angular distributions (PADs) which strongly depend on the polarization state of the ionizing electric field [17, 18]. To record and study such PADs, one of the most powerful tool is the COLd Target Recoil Ion Momentum Spectrometer (COLTRIMS) Reaction Microscope (ReMi), called here briefly as C-ReMi [19]. In addition, by recording PADs we are also able to track the radiation-induced charge

migrations and chemical dynamics in real time, which shows the versatility of this equipment in the research of ultrafast physical phenomena [20, 21].

Another technique to measure the polarization of the XUV radiation utilizes the sensitivity of the reflection and refraction of the materials to the polarization state of incident electromagnetic fields [22]. XUV polarimeters take advantage of this effect, however, they can operate effectively only in reflection geometry, as this radiation is significantly attenuated in a short propagation length in all the materials known so far. An XUV polarimeter can be experimentally realized in several ways: mono-stage in a four-mirror configuration [23], double-staged with three reflections [24, 25]. One can also extract information about polarization with only one stage consisting of three mirrors [26, 27], although this latter configuration is not sufficient to determine the full polarization ellipse like in the case of the setup at the ELI Beamlines facility [28]. In addition, polarimeters are also used to measure the reflectance and ellipsometric parameters of different materials, but in this case the experimental conditions are the opposite: the polarization state of the applied radiation is known, and the material response needs to be measured [27, 29, 30]. Prior to such measurements, the characteristics of the polarimeter must be determined in almost every case [31, 32]. To investigate the fundamental properties of the materials, the combination of synchrotron radiation with reflectometers is the most widespread method [33–35].

Considering polarimetry, some research has focused on the simultaneous measurement of the polarization state with different measurement techniques. Takahashi and co-workers conducted the first comparative study using a multilayer polarizer and a velocity imaging photoelectron analyzer [36]. With a similar goal, the polarization state of only two harmonic orders produced in a liquid phase target was investigated with a velocity map imaging spectrometer supported with a single-stage, four-reflection-based polarimeter [37]. Furthermore, quasi-cw synchrotron radiation has also been characterized simultaneously with a double-stage, triple-reflection polarimeter and a C-ReMi device [38].

In this work, we present the complete reconstruction of different polarization states of a broadband XUV source with a double-stage, three-reflection-based polarimeter (optical method), and in parallel we determine the material constants of the reflective gold layers on the optics used in the polarimeter. In addition, we measured the polarization ellipse of the broadband XUV radiation with C-ReMi equipment (non-optical technique) in support of the results obtained with the polarimeter. With these achievements, we extend spectroscopic ellipsometry—used in a wide frequency range [39]—to the XUV using a table-top setup. This information is extremely important in the explosive development of semiconductor lithography [40] as well as in time- and angle-resolved photoelectron spectroscopy [41, 42], which require well-characterized steering optics in this spectral region. By replacing one of the steering optics in our polarimeter, any kind of reflective layer or bulk material can be characterized in a broad photon energy range. Furthermore, the combination of high-resolution ellipsometry with pump-probe capabilities of the beamline allows the validation of the Kramers–Kronig relations on the attosecond time scale [43]. Additionally, the complex time-dependent polarization state of attosecond pulse trains or an isolated attosecond pulse can also be determined [44–47], which is a prerequisite for the investigation of chiral phenomena [48, 49] and magnetic circular dichroism [50, 51]. Simultaneously, time-dependent chiro-optical processes can be studied in the ReMi with high momentum and time resolution by detailed investigations of photoion and photoelectron fragments [50, 52]. Moreover, the measurement of the complete polarization state can provide deeper insight into the atomic processes during harmonic generation on the femtosecond time scale through attosecond spatial interferometry [53].

2. Methods

We used the Stokes formalism for the description of the polarization state of radiation [54, 55], about which more details can be found in section 1 of Supplementary Material (SM). Here we only note that the retrieved quantities are the normalized Stokes parameters (S_1', S_2', S_3'), as they unequivocally describe the complete polarization ellipse of any electromagnetic radiation.

The experiments were carried out on the High Repetition rate laser system-based gas HHG beamline for Gas targets (HR Gas) at the Extreme Light Infrastructure Attosecond Light Pulse Source (ELI ALPS) Research Facility [56, 57]. The beamline was driven by the HR Alignment laser source during these experiments [58], emitting ultrashort pulses at 10 kHz repetition rate with 1 mJ pulse energy, generating broadband XUV radiation in the $18-44$ eV photon energy range via HHG in a gas cell target [59]. The beamline is standardly equipped with the C-ReMi and the double-stage, three-reflection-based polarimeter, allowing simultaneous measurements on the polarization state of the XUV radiation [60] (more information about the beamline geometry can be seen in section 2 of SM). The full polarization characterization of the HHG-based XUV source was carried out in two orthogonal, linear polarization states. To change the experimental conditions, we simply rotated the polarization plane of the driving

laser field by using a broadband half-wave plate before the harmonic generation point, which resulted in orthogonally polarized high-harmonics in the two conditions.

Since the measured signals are completely different in the optical and the non-optical methods, significantly different evaluation processes must be applied for the extraction of the normalized Stokes parameters. For the sake of brevity, here we only summarize the main aspects of evaluation of the recorded datasets. The detailed description of the evaluation steps can be found in section 3 of SM. Based on data from the PADs, measured with the C-ReMi, we can obtain only limited information about the polarization state of the ionizing radiation, i.e. the Stokes parameters S_1' and S_2' can be determined in the current configuration. In addition, the tilting angle (θ_0) of the polarization ellipse can be reconstructed (see section 3.1 of SM), and the reconstruction of S_3' would be available with specialized targets in C-ReMi (see, for example, [61]). In case of data acquisition with the polarimeter, due to the polarization dependence of the complex reflection coefficients of the optics used, the transmitted intensity varies with the rotational angles of the stages, resulting in a three-dimensional surface of the intensity variations, called Malus surface [62]. By performing three-dimensional surface fitting we determined all Stokes parameters (S_1', S_2', S_3') of the input radiation together with the $\psi_{1,\mathrm{tot}}$, $\psi_{2,\mathrm{tot}}$ and Δ_1 ellipsometric parameters of the reflective gold thin films evaporated on the optics used in the polarimeter (see section 3.2 of SM) [62].

3. Discussion

The normalized Stokes parameters measured in the two orthogonally polarized measurement conditions are presented in figure 1: figure 1(a) shows a horizontally- and figure 1(b) represents a vertically polarized condition. The solid black curves show the generated harmonic spectra in both cases. The full dots present variations of the normalized Stokes parameters in the $18-44$ eV photon energy range. The corresponding error bars represent the uncertainty of their reconstruction, resulting from the imperfections of surface fitting to the recorded Malus surfaces. The dotted horizontal lines indicate the values of the photon energy-integrated normalized Stokes parameters, based on the spectrometer signal.

We note here that there are additional peaks in the high-harmonic spectra neighboring harmonics 15 and 17 (18 eV and 20.4 eV, respectively) in both measurement conditions, which are the cut-off harmonics caused by the second-order diffraction of the grating used in the spectrometer. However, this second-order diffraction does not deteriorate the reconstruction of the polarization state of lower-orders because these peaks do not overlap completely with the peaks from the first diffraction order, and can be filtered out during data evaluation. We also note here that a perfectly linearly polarized field with horizontal and vertical polarizations should have $S_1' = 1$ and $S_1' = -1$, respectively, with other Stokes parameters being zero. The fact that $S_2' \neq 0$ in both cases only means that the angle of polarization was not perfectly aligned with the vertical/horizontal axes of the polarimeter. Based on the S_2' (and S_1') values measured with the polarimeter, the actual polarization angle was $\sim 6^\circ$ and $\sim 2^\circ$ rotated with respect to the polarimeter axis, for the cases shown in figures 1 (a) and (b). Overall, in our generation conditions the normalized Stokes parameter S_1' and S_2' vary slightly with photon energy in the plateau region of the high-harmonic spectrum, while in the vicinity of the cut-off they show more pronounced variations, most profoundly visible in case of S_3'. This observation resembles the results summarized in the work of Antoine *et al* [63], as they observed differences in the polarization state of the harmonics located in the plateau and cut-off regions. With our method, however, the full polarization state can be reconstructed, while in [64] S_3' could only be deduced indirectly by assuming fully polarized light, and the information on the sign of ellipticity was not possible to reconstruct. Our results suggest that the deviation from perfectly linearly polarized HHG radiation is not caused by an unpolarized component, but by the presence of a circularly polarized harmonic field. This is particularly interesting in view of the proposal [64], where the amplitudes and phases of the Fourier components of the single-atom dipole moment vary rapidly with the laser intensity, and as a result, only partially polarized radiation can be measured experimentally due to spatial averaging across the different intensity sections of the laser beam cross section. While our measurement methods allow for a clear distinction between partially and elliptically polarized light, the detailed analysis and interpretation of measured Stokes parameters lie outside the scope of this work, as polarization properties of HHG radiation depend strongly both on single-atom and macroscopic conditions.

Because the geometry of the HR Gas beamline is designed to enable researchers to conduct measurements simultaneously with the XUV polarimeter and the C-ReMi, we determined the polarization state of the XUV radiation by using the C-ReMi device as well. Thereby, we can benchmark the optical method with a non-optical measurement technique, applying a significantly different measurement and data evaluation process (see sections 2.3 and 3.1 of SM). The results obtained are also presented in figure 1 with light blue ($S_1'^{\mathrm{ReMi}}$) and dark red ($S_2'^{\mathrm{ReMi}}$) diamond symbols together with the corresponding

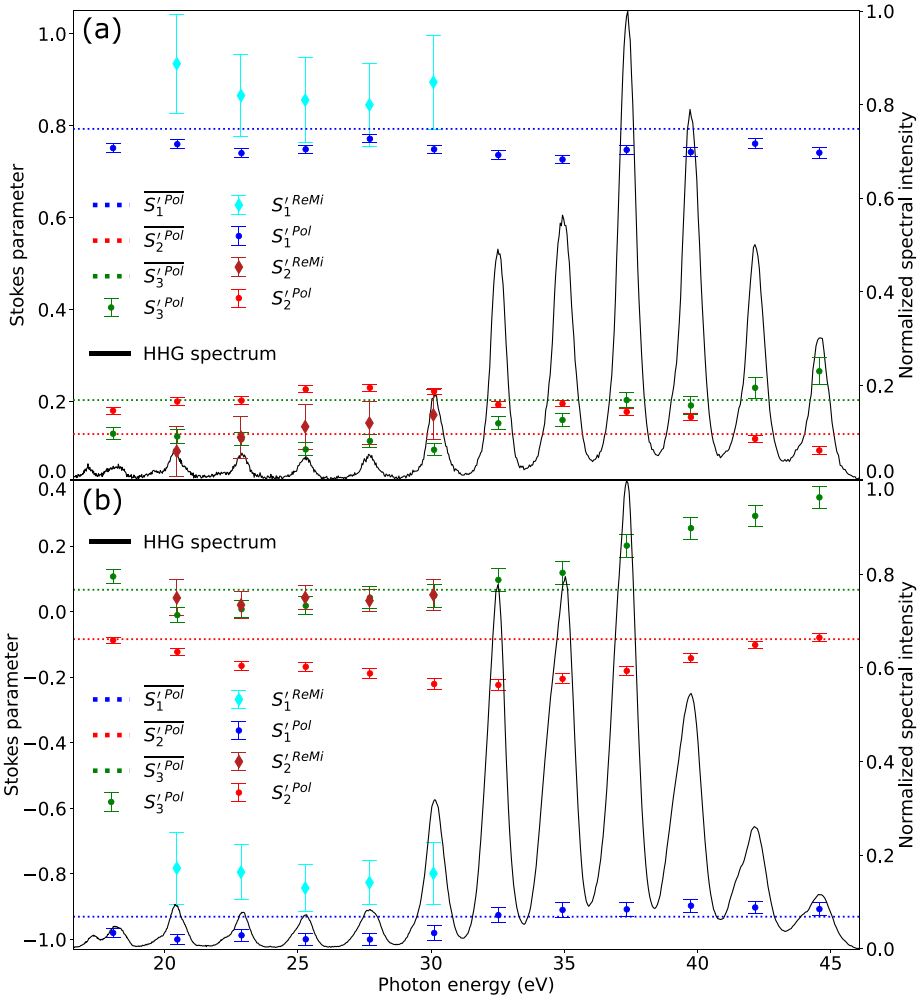

Figure 1. Reconstruction of the polarization state of the harmonic-generation-based XUV source is presented in case of (a) a horizontally and (b) vertically polarized driving laser field. The solid black curves are the produced HHG spectra and the full dots present the variations of the normalized Stokes parameters in the covered $18-44$ eV photon energy range measured with the XUV polarimeter. The indicated error bars are the uncertainty of their reconstruction. The horizontal dotted lines represent the values of the photon energy integrated, normalized Stokes parameters calculated based on the spectrometer signal. For comparison the normalized Stokes parameters retrieved from the PADs recorded with the C-ReMi are also presented with diamond symbols analogously with error bars.

reconstruction uncertainties in both experimental conditions. The target gas, injected into the C-ReMi, was Ar, an optically inactive gas, which did not allow reconstruction of the helicity of XUV radiation, namely the normalized Stokes parameter S_3'. Apart from this, the parameters $S_1'^{\mathrm{ReMi}}$ and $S_2'^{\mathrm{ReMi}}$ were successfully retrieved from the PADs in the $20-30$ eV photon energy range. The detectable spectral region depends on the geometry of the spectrometer and the electric and magnetic fields were chosen to allow a sufficiently high kinetic energy resolution for clearly distinguishing photoelectron peaks originating from different harmonics. The technique is scalable in terms of photon energy by selecting target materials with different ionization potentials and photoionization cross sections. At first glance this method looks less accurate compared with the results of the polarimeter. However, the wider error bars in this case are due to the lack of statistics, which could be substantially improved with a higher repetition rate laser source or longer data acquisition that would further improve the match with the results obtained with the polarimeter. We also note that the measurements with the polarimeter and the C-ReMi show differences in the values of S_1' and S_2'. These, however, can be explained with the non-parallel alignment of the reference axes of the two devices. From the datasets presented in figure 1 (a) and (b), we consistently get a value of $\sim 5°$ for the angle that the two vertical (or horizontal) axes of the two devices make with respect to each other. The C-ReMi measurements also confirm that in the two measurements the horizontal and vertical (p- and s-polarized) fields presented in figure 1 (a) and (b) actually close an angle of around 86° instead of 90°.

In addition to the robust determination of the complete polarization state of the XUV source with two independent metrology, the ellipsometric parameters, i.e. the characteristics of the uncoated gold

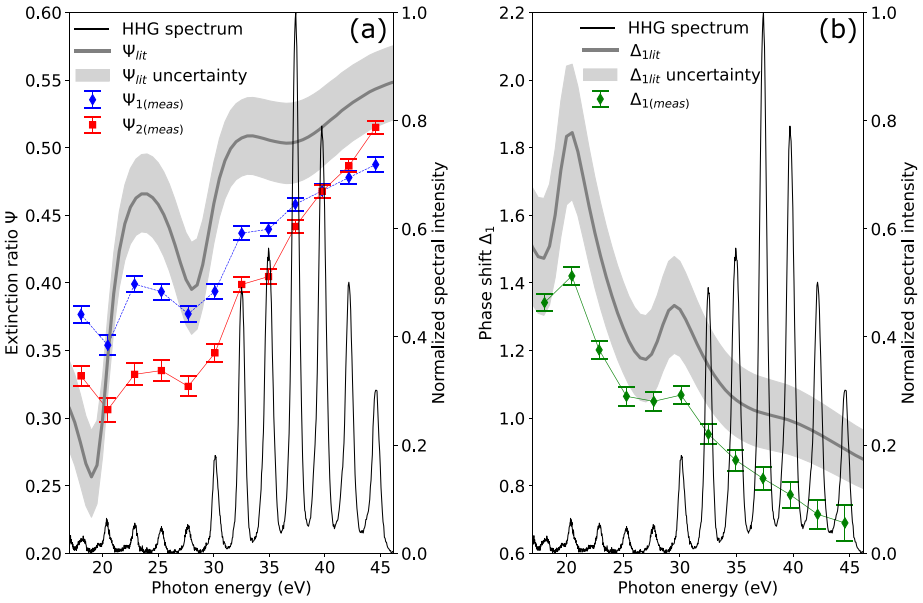

Figure 2. Ellipsometric parameters of the uncoated gold mirrors implemented in the double-stage, three-reflection-based XUV polarimeter. (a) Extinction ratios $\psi_{1(\mathrm{meas})}$ (blue diamonds) and $\psi_{2(\mathrm{meas})}$ (red squares) of the individual polarimeter stages and (b) phase difference $\Delta_{1(\mathrm{meas})}$ (green diamonds) introduced between the two polarization components. In both figures the black curves represent the harmonic spectra to be generated. The solid gray curves are the corresponding data taken from the latest experimental results found in the literature. The light gray shaded area shows the variation of the ellipsometric parameters, by changing the angle of incidence to the surface of the first mirror in the polarimeter stage by 1°.

mirrors installed in the polarimeter stages—replaceable with an arbitrary sample—are also determined from the same dataset (see section 3.2 of SM). To be more specific, the extinction ratios $\psi_{1,\mathrm{tot}}$ and $\psi_{2,\mathrm{tot}}$ of the individual polarimeter stages, and the phase shift Δ_1 introduced between the two orthogonal polarization components in the first polarimeter stage are also retrieved with high accuracy in the $18-44\,\mathrm{eV}$ photon energy range from the same surface fitting carried out for the reconstruction of the normalized Stokes parameters (see SM section 3.2). The results obtained are presented in figure 2 together with the accuracy of the retrieval. Figure 2(a) shows the reconstructed extinction ratios $\psi_{1(\mathrm{meas})}$ (blue diamonds) and $\psi_{2(\mathrm{meas})}$ (red squares), and in figure 2(b) the measured phase shift $\Delta_{1(\mathrm{meas})}$ (green diamonds) are plotted. In both figures, the black curves show the produced high-harmonic spectrum. For the sake of comparability, we present the latest experimental results found in the literature, which focused on the determination of the material constants of bulk gold material (solid gray curves), as they have the highest resolution in this photon energy range [65]. As there are no significant differences in the tendencies of such material constants in case of bulk materials and thin films (see section 4 of SM), we consider this reference to be adequate for comparison. The light gray shaded area represents the variation of the ellipsometric parameters, by changing the angle of incidence (AOI) to the surface of the first mirror in the polarimeter stage by 1°. This broad area shows that the precise alignment of the experimental setup substantially affects the material constants to be reconstructed (but it would not affect changes measured in a pump-probe scheme). In our configuration, the nominal AOI of the three mirrors in each polarimeter stage is designed to be $80°-70°-80°$, respectively, and these values were used in the calculations of the solid gray curves in figure 2. The ellipsometric parameters measured in this work slightly differ from the reference data, however, the aging of the uncoated gold layers evaporated on the mirrors used in the polarimeter stages can lead to such deviations from the reference curve. In addition, both the experimentally measured and empirical values of these parameters found in the literature show a large variations as presented in section 4 of SM, which supports that the optical constants of gold layers are strongly influenced by the measurement conditions and the quality of the surface. All in all, these material constants were successfully retrieved, extending the experimental results to the ellipsometric parameters of thin gold layers. We also note here that the measurement precision of the ellipsometric angles provided by the polarimeter in the photon energy range to be measured should allow for tracking ultrafast processes in matter, just like in the visible regime [66]. Also, since HHG with short pulses can provide a continuous spectrum [67], the photon energy resolution can be increased up to the resolution limit of the spectrometer used, resembling more the ellipsometric measurements known from the optical regime [39].

4. Conclusions

We demonstrated successful measurements on the full polarization state of a HHG-based XUV source under two orthogonally polarized measurement conditions covering the $18-44\,\mathrm{eV}$ photon energy range. Reconstruction of the complete polarization ellipse of high-harmonics is carried out simultaneously with an optical (polarimeter) and a non-optical (ReMi) measurement technique, which is unprecedented in such a broad spectral region by using a harmonic-based XUV source.

In addition, we determined the ellipsometric parameters of the thin gold layers evaporated on the reflective optics installed in the polarimeter stages with the same set of measurements in the $18-44\,\mathrm{eV}$ spectral region. To the best of our knowledge, the measurement of these material constants of thin film materials using a table-top XUV source is reported for the first time. Until now, these investigations have been conducted using synchrotron radiation in combination with reflectometers [33–35]. A remarkable advantage of our setup and solution is that due to the parallel polarimetry and ellipsometry, the polarization of the light does not need to be characterized in advance to carry out ellipsometry.

These results lay the foundations of high-resolution ellipsometry measurements on any kind of reflective layer or bulk material with sufficient reflection for XUV radiation produced by broadband HHG-based light sources. This possibility is of great importance in semiconductor lithography [40] or in time- and angle-resolved photoelectron spectroscopy [41, 42], where well-characterized steering optics are required in this spectral range. Furthermore, by replacing steering optics in the polarimeter, the presented methodology can be expanded to other photon energies in a broad spectral range. In addition, simultaneous measurement with the polarimeter and the C-ReMi in a pump-probe scheme allows the determination of the complex time-dependent polarization state of attosecond pulses [44–46], and the investigation of chiral phenomena [48, 49, 51] or time-dependent chiro-optical processes [50, 52] on the attosecond timescale.

Data availability statement

All data that support the findings of this study are included within the article (and any supplementary files).

Acknowledgments

The ELI ALPS project (GINOP-2.3.6-15-2015-00001) is supported by the European Union and co-financed by the European Regional Development Fund. The work of BM was supported by the Bolyai Janos Research Scholarship of the Hungarian Academy of Sciences. The experimental setup was implemented with support from the IMPULSE project, which received funding from the European Union Framework Programme for Research and Innovation Horizon 2020.

Author contributions

Lénárd Gulyás Oldal 0000-0003-2852-9945
Conceptualization (equal), Investigation (equal), Methodology (equal), Project administration (equal), Resources (equal), Software (equal), Validation (equal), Visualization (equal), Writing – original draft (equal), Writing – review & editing (equal)

Barnabás Gilicze 0000-0002-5893-8144
Methodology (equal), Resources (equal)

Tamás Bartyik 0000-0003-1608-4889
Methodology (equal), Resources (equal)

Dániel Kiss 0009-0003-0709-0029
Methodology (supporting), Resources (supporting)

Michele Devetta 0000-0002-3806-3475
Methodology (equal), Resources (equal)

Gabriele Zeni 0000-0003-3972-1991
Resources (supporting)

Fabio Frassetto 0000-0001-5528-1995
Resources (equal), Writing – review & editing (supporting)

Luca Poletto 0000-0002-0914-0531
Resources (equal), Writing – review & editing (supporting)

Tamás Csizmadia 0000-0001-5969-9846
Conceptualization (equal), Methodology (equal), Project administration (equal), Resources (equal), Software (equal), Supervision (equal), Validation (equal), Visualization (equal), Writing – original draft (equal), Writing – review & editing (equal)

Balázs Major 0000-0001-5981-340X
Conceptualization (equal), Methodology (equal), Project administration (equal), Resources (equal), Supervision (equal), Validation (equal), Writing – original draft (equal), Writing – review & editing (equal)

References

[1] Ferré A *et al* 2015 A table-top source based on high-harmonic generation produces bright, coherent, quasi-circular pulses of extreme ultraviolet light for probing chiral molecules *Nat. Photon.* **9** 93–98
[2] Radu I *et al* 2011 Transient ferromagnetic-like state mediating ultrafast reversal of antiferromagnetically coupled spins *Nature* **472** 205–8
[3] Reduzzi M *et al* 2015 Advances in high-order harmonic generation sources for time-resolved investigations *J. Electron Spectrosc. Relat. Phenom.* **204** 257–68
[4] Chatziathanasiou S, Kahaly S, Skantzakis E, Sansone G, Lopez-Martens R, Haessler S, Varju K, Tsakiris G D, Charalambidis D and Tzallas P 2017 Generation of attosecond light pulses from gas and solid state media *Photonics* **4** 26
[5] Winterfeldt C, Spielmann C and Gerber G 2008 Colloquium: optimal control of high-harmonic generation *Rev. Mod. Phys.* **80** 117–40
[6] Teubner U and Gibbon P 2009 High-order harmonics from laser-irradiated plasma surfaces *Rev. Mod. Phys.* **81** 445–79
[7] Luu T T, Yin Z, Jain A, Gaumnitz T, Pertot Y, Ma J and Wörner H J 2018 Extreme–ultraviolet high–harmonic generation in liquids *Nat. Commun.* **9** 3723
[8] Ghimire S, DiChiara A D, Sistrunk E, Agostini P, DiMauro L F and Reis D A 2011 Observation of high-order harmonic generation in a bulk crystal *Nat. Phys.* **7** 138–41
[9] Corkum P B 1993 Plasma perspective on strong field multiphoton ionization *Phys. Rev. Lett.* **71** 1994–7
[10] Salières P, L'Huillier A and Lewenstein M 1995 Coherence control of high-order harmonics *Phys. Rev. Lett.* **74** 3776–9
[11] Gulyás Oldal L, Csizmadia T, Ye P, Harshitha N G, Zaïr A, Kahaly S, Varjú K, Füle M and Major B 2020 Generation of high-order harmonics with tunable photon energy and spectral width using double pulses *Phys. Rev. A* **102** 013504
[12] Gulyás Oldal L *et al* 2021 All-optical experimental control of high-harmonic photon energy *Phys. Rev. Appl.* **16** L011001
[13] Huang P-C *et al* 2018 Polarization control of isolated high-harmonic pulses *Nat. Photon.* **12** 349–54
[14] Lutman A A *et al* 2016 Polarization control in an x-ray free-electron laser *Nat. Photon.* **10** 468–72
[15] Chang K-Y, Huang L-C, Asaga K, Tsai M-S, Rego L, Huang P-C, Mashiko H, Oguri K, Hernández-García C and Chen M-C 2021 High-order nonlinear dipole response characterized by extreme ultraviolet ellipsometry *Optica* **8** 484–92
[16] Allaria E *et al* 2014 Control of the polarization of a vacuum-ultraviolet, high-gain, free-electron laser *Phys. Rev. X* **4** 041040
[17] Lörch H, Scherer N, Kerkau T and Schmidt V 1999 VUV light polarization measured by coincidence electron spectrometry *J. Phys. B* **32** L371
[18] Li W B *et al* 2007 Photoemission in the molecular frame induced by soft x-ray elliptically polarized light *J. Electron Spectrosc. Relat. Phenom.* **156-158** 30–37
[19] Ullrich J, Moshammer R, Dorn A, Dörner R, Schmidt L P H and Schmidt-Böcking H 2003 Recoil-ion and electron momentum spectroscopy: reaction-microscopes *Rep. Prog. Phys.* **66** 1463
[20] Dörner R, Weber T, Weckenbrock M, Staudte A, Hattass M, Schmidt-Böcking H, Moshammer R and Ullrich J 2002 Multiple ionization in strong laser fields *Advances In Atomic, Molecular and Optical Physics* vol 48, ed B Bederson and H Walther (Academic) pp 1–34
[21] Schmidt-Böcking H, Ullrich J, Dörner R and Cocke C L 2021 The COLTRIMS reaction microscope—the spyhole into the ultrafast entangled dynamics of atomic and molecular systems *Ann. Phys.* **533** 2100134
[22] Chiu M-H, Lee J-Y and Su D-C 1999 Complex refractive-index measurement based on Fresnel's equations and the uses of heterodyne interferometry *Appl. Opt.* **38** 4047–52
[23] Svoboda V, Yin Z, Luu T T and Wörner H J 2021 Polarization measurements of deep- to extreme-ultraviolet high harmonics generated in liquid flat sheets *Opt. Express* **29** 30799–808
[24] Koide T, Shidara T, Yuri M, Kandaka N, Yamaguchi K and Fukutani H 1991 Elliptical-polarization analyses of synchrotron radiation in the 5-80-eV region with a reflection polarimeter *Nucl. Instrum. Methods Phys. Res. A* **308** 635–44
[25] Nahon L and Alcaraz C 2004 SU5: a calibrated variable-polarization synchrotron radiation beam line in the vacuum-ultraviolet range *Appl. Opt.* **43** 1024–37
[26] Cubric D, Cooper D R, Lopes M C A, Bolognesi P and King G C 1999 Polarization measurements in the VUV region of synchrotron radiation *Meas. Sci. Technol.* **10** 554
[27] Zuppella P, Samparisi F, Frassetto F, Rigato V, Campostrini M and Poletto L 2022 Measurement of the ellipsometric parameters of thin graphene layers in the extreme ultraviolet *J. Phys. Conf. Ser.* **2380** 012079
[28] Espinoza S *et al* 2020 Characterization of the high harmonics source for the VUV ellipsometer at ELI Beamlines *J. Vac. Sci. Technol. B* **38** 024005
[29] Brimhall N, Turner M, Herrick N, Allred D D, Turley R S, Ware M and Peatross J 2008 Extreme-ultraviolet polarimeter utilizing laser-generated high-order harmonics *Rev. Sci. Instrum.* **79** 103108

[30] Brimhall N, Heilmann N, Ware M and Peatross J 2009 Polarization-ratio reflectance measurements in the extreme ultraviolet *Opt. Lett.* **34** 1429–31
[31] Kandaka N, Yuri M, Fukutani H, Koide T and Shidara T 1992 Ellipsometrical determination of the optical constants of gold in the vacuum ultraviolet region *Rev. Sci. Instrum.* **63** 1450–3
[32] Schäfers F *et al* 1999 Soft-x-ray polarimeter with multilayer optics: complete analysis of the polarization state of light *Appl. Opt.* **38** 4074–88
[33] Wolf R, Birken H-G, Blessing C and Kunz C 1994 Optical constants of gold in the soft-x-ray region from reflection and transmission measurements *Appl. Opt.* **33** 2683–94
[34] Yanagihara M, Cao J, Yamamoto M, Arai A, Nakayama S, Mizuide T and Namioka T 1991 Optical constants of very thin gold films in the soft x-ray region *Appl. Opt.* **30** 2807–14
[35] Windt D L, Cash W C, Scott M, Arendt P, Newnam B, Fisher R F and Swartzlander A B 1988 Optical constants for thin films of Ti, Zr, Nb, Mo, Ru, Rh, Pd, Ag, Hf, Ta, W, Re, Ir, Os, Pt and Au from 24 Å to 1216 Å *Appl. Opt.* **27** 246–78
[36] Takahashi M, Hatano T, Ejima T, Kondo Y, Saito K, Watanabe M, Kinugawa T and Eland J 2003 Polarization measurements of laboratory VUV light: a first comparison between multilayer polarizers and photoelectron angular distributions *J. Electron. Spectrosc. Relat. Phenom.* **130** 79–84
[37] Svoboda V, Waters M D J, Zindel D and Wörner H J 2022 Generation and complete polarimetry of ultrashort circularly polarized extreme-ultraviolet pulses *Opt. Express* **30** 14358–67
[38] Veyrinas K, Elkharrat C, Poullain S M, Saquet N, Dowek D, Lucchese R R, Garcia G A and Nahon L 2013 Complete determination of the state of elliptically polarized light by electron-ion vector correlations *Phys. Rev. A* **88** 063411
[39] Hilfiker J N, Bungay C L, Synowicki R A, Tiwald T E, Herzinger C M, Johs B, Pribil G K and Woollam J A 2003 Progress in spectroscopic ellipsometry: applications from vacuum ultraviolet to infrared *J. Vac. Sci. Technol. A* **21** 1103–8
[40] Kazazis D, Santaclara J G, van Schoot J, Mochi I and Ekinci Y 2024 Extreme ultraviolet lithography *Nat. Rev. Methods Primers* **4** 84
[41] Dakovski G L, Li Y, Durakiewicz T and Rodriguez G 2010 Tunable ultrafast extreme ultraviolet source for time- and angle-resolved photoemission spectroscopy *Rev. Sci. Instrum.* **81** 073108
[42] Sabbar M, Heuser S, Boge R, Lucchini M, Gallmann L, Cirelli C and Keller U 2014 Combining attosecond XUV pulses with coincidence spectroscopy *Rev. Sci. Instrum.* **85** 103113
[43] Leshchenko V, Hageman S J, Cariker C, Smith G, Camper A, Talbert B K, Agostini P, Argenti L and DiMauro L F 2023 Kramers–Kronig relation in attosecond transient absorption spectroscopy *Optica* **10** 142–6
[44] Ansari I N, Hofmann C, Medišauskas L, Lewenstein M, Ciappina M F and Dixit G 2021 Controlling polarization of attosecond pulses with plasmonic-enhanced bichromatic counter-rotating circularly polarized fields *Phys. Rev. A* **103** 013104
[45] Dorney K M *et al* 2019 Controlling the polarization and vortex charge of attosecond high-harmonic beams via simultaneous spin—orbit momentum conservation *Nat. Photon.* **13** 123–30
[46] Milošević D B and Becker W 2000 Attosecond pulse trains with unusual nonlinear polarization *Phys. Rev. A* **62** 011403(R)
[47] Csizmadia T, Gulyás Oldal L, Gilicze B, Kiss D, Bartyik T, Varjú K, Kahaly S and Major B 2025 Active stabilization for ultralong acquisitions in an attosecond pump–probe beamline *APL Photonics* **10** 080803
[48] Ayuso D, Ordonez A F and Smirnova O 2022 Ultrafast chirality: the road to efficient chiral measurements *Phys. Chem. Chem. Phys.* **24** 26962–91
[49] Powis I 2000 Photoelectron circular dichroism of the randomly oriented chiral molecules glyceraldehyde and lactic acid *J. Chem. Phys.* **112** 301–10
[50] Fehre K *et al* 2021 Fourfold differential photoelectron circular dichroism *Phys. Rev. Lett.* **127** 103201
[51] Zayko S, Kfir O, Heigl M, Lohmann M, Sivis M, Albrecht M and Ropers C 2021 Ultrafast high-harmonic nanoscopy of magnetization dynamics *Nat. Commun.* **12** 6337
[52] Hennecke M *et al* 2024 Ultrafast opto-magnetic effects in the extreme ultraviolet spectral range *Commun. Phys.* **7** 191
[53] Carpeggiani P *et al* 2017 Vectorial optical field reconstruction by attosecond spatial interferometry *Nat. Photon.* **11** 383–9
[54] Jones R C 1941 A new calculus for the treatment of optical systems: I. description and discussion of the calculus *J. Opt. Soc. Am.* **31** 488–93
[55] Stokes G G 1851 On the composition and resolution of streams of polarized light from different sources *Trans. Camb. Phil. Soc.* **9** 399
[56] Ye P *et al* 2020 Attosecond pulse generation at ELI-ALPS 100 kHz repetition rate beamline *J. Phys. B* **53** 154004
[57] Ye P *et al* 2022 High-flux 100 kHz attosecond pulse source driven by a high-average power annular laser beam *Ultrafast Sci.* **2022** 9823783
[58] Gilicze B *et al* 2025 Repetition-rate-independent post-compression to achieve CEP stable few-cycle laser pulses *High Power Laser Sci. Eng.* 1–20
[59] Filus Z, Ye P, Csizmadia T, Grósz T, Gulyás Oldal L, De Marco M, Füle M, Kahaly S, Varjú K and Major B 2022 Liquid-cooled modular gas cell system for high-order harmonic generation using high average power laser systems *Rev. Sci. Instrum.* **93** 073002
[60] Shirozhan M *et al* 2024 High-repetition-rate attosecond extreme ultraviolet beamlines at ELI ALPS for studying ultrafast phenomena *Ultrafast Sci.* **4** 0067
[61] Barreau L *et al* 2018 Evidence of depolarization and ellipticity of high harmonics driven by ultrashort bichromatic circularly polarized fields *Nat. Commun.* **9** 4727
[62] Frassetto F, Zuppella P, Samparisi F, Fabris N and Poletto L 2019 Transition metal coatings for reflection polarimeters in the 50-100 eV region *X-Ray Free-Electron Lasers: Advances in Source Development and Instrumentation Proc. SPIE* **11038** 110380M
[63] Antoine P, Carré B, L'Huillier A and Lewenstein M 1997 Polarization of high-order harmonics *Phys. Rev. A* **55** 1314–24
[64] Antoine P, L'Huillier A, Lewenstein M, Salières P and Carré B 1996 Theory of high-order harmonic generation by an elliptically polarized laser field *Phys. Rev. A* **53** 1725–45
[65] Werner W S M, Glantschnig K and Ambrosch-Draxl C 2009 Optical constants and inelastic electron-scattering data for 17 elemental metals *J. Phys. Chem. Ref. Data* **38** 1013–92
[66] Budai J, Pápa Z, Petrik P and Dombi P 2022 Ultrasensitive probing of plasmonic hot electron occupancies *Nat. Commun.* **13** 6695
[67] Ishii N, Kaneshima K, Kitano K, Kanai T, Watanabe S and Itatani J 2014 Carrier-envelope phase-dependent high harmonic generation in the water window using few-cycle infrared pulses *Nat. Commun.* **5** 3331